

# W Charge Asymmetry at CDF II

## Fermilab Summer Program: Final Report

VALENTINA VECCHIO  
*Università degli Studi Roma Tre*  
September 25, 2015

---

### Introduction

In this report I describe my work in the Summer School Program at Fermilab in 2015.

During the period that goes from the 27th of July and the 25th of September I worked with CDF group under the supervision of **Dr. Willis Sakumoto**. I learned about the CDF detector, its component and  $p\bar{p}$  collisions at Tevatron (Section 1).

I studied the production and decay of W boson, focusing my attention on the  $W \rightarrow e\nu_e$  channel and all its associated backgrounds.

Then I moved to W Asymmetry in charge, how to do this measurement and why it's so important. (Section 2).

In Section 3 all details of preliminar analisys are described and in Section 4 new good quality plug tracks studies are reported. At last asymmetry plot and conclusion are reported (Section 5) with a brief description of charge misidentification starting studies.

## Contents

<b>1</b>	<b>Tevatron &amp; CDF Experiment</b>	<b>3</b>
1.1	Tevatron . . . . .	3
1.2	The CDF II Detector [1] . . . . .	4
1.2.1	Tracking System . . . . .	5
1.2.2	Calorimeter System . . . . .	6
1.2.3	Muon Systems . . . . .	6
<b>2</b>	<b>W boson</b>	<b>7</b>
2.1	Production and decay . . . . .	7
2.2	Asymmetries . . . . .	8
2.3	Signal and backgrounds . . . . .	10
<b>3</b>	<b>Data Analysis</b>	<b>11</b>
3.1	Samples . . . . .	11
3.2	General event selections [2] [3] [4] . . . . .	12
3.2.1	Central events . . . . .	12
3.2.2	Plug Events . . . . .	13
<b>4</b>	<b>Plug region special analysis</b>	<b>14</b>
4.1	Good Quality Track selection . . . . .	15
4.1.1	Track quality parameters and benchmark distributions	15
<b>5</b>	<b>Asymmetry plots and results</b>	<b>17</b>
5.1	Charge Misidentification [5] . . . . .	19
<b>6</b>	<b>Conclusions</b>	<b>21</b>

# 1 Tevatron & CDF Experiment

## 1.1 Tevatron

Tevatron is a  $p\bar{p}$  collider and it currently holds the title of the second highest energy particle collider in the world. Residing at Fermi National Accelerator Laboratory (Batavia), the Tevatron accelerated and stored beams of protons and antiprotons traveling in opposite directions around an underground ring of 6,86 Km in circumference at almost the speed of light before colliding them at the center of two detectors.

The acceleration occurs in a number of stages exposed in Figure 1.

The first stage is the 750 keV Cockcroft-Walton pre-accelerator, which

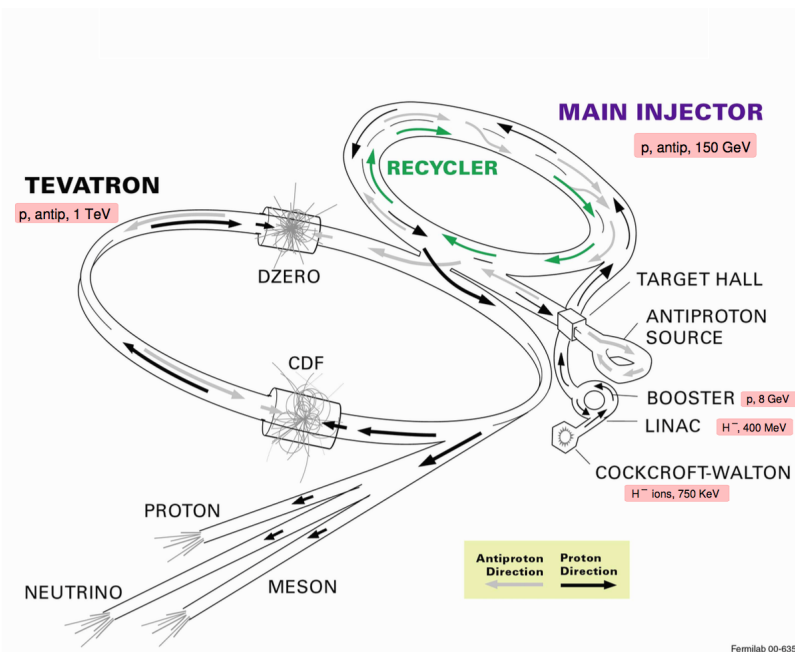


Figure 1: Fermilab's Accelerator Chain

ionizes hydrogen gas and accelerates the negative ions created using a positive voltage. Then ions pass into the 150 meter long linear accelerator (Linac) which uses oscillating electrical fields to accelerate the ions to 400 MeV. After this stage ions pass through a carbon foil, to remove the electrons, and the charged protons then move into the Booster. The Booster is a small circular synchrotron, around which the protons pass up to 20,000 times to attain an energy of around 8 GeV. From the Booster the particles pass into the Main Injector, which was completed in 1999. It can accelerate protons up to 150 GeV; it can produce 120 GeV protons for antiproton creation; it can increase antiproton energy to 150 GeV and it can inject protons or

antiprotons into the Tevatron.

The antiprotons are created by the Antiproton Source: 120 GeV protons are collided with a nickel target producing a range of particles including antiprotons which can be collected and stored in the accumulator ring. The ring can then pass the antiprotons to the Main Injector. The Tevatron can accelerate the particles from the Main Injector up to 980 GeV. The protons and antiprotons are accelerated in opposite directions, crossing paths in the CDF and DZero detectors to collide at 1.96 TeV. To hold the particles on track the Tevatron uses 774 niobium-titanium superconducting dipole magnets cooled in liquid helium producing 4.2 T. The field ramps over about 20 seconds as the particles are accelerated. Another 240 NbTi quadrupole magnets are used to focus the beam.

## 1.2 The CDF II Detector [1]

CDF II is a general purpose solenoidal detector for the study of  $p\bar{p}$  collisions at the Fermilab Tevatron Collider. It worked from 1985 to 2011. In the last Run it collected around  $10fb^{-1}$  integrated luminosity.

The detector is shown in an elevation view in Figure 2.

Tracking systems are contained in a superconducting solenoid, 1.5 m in

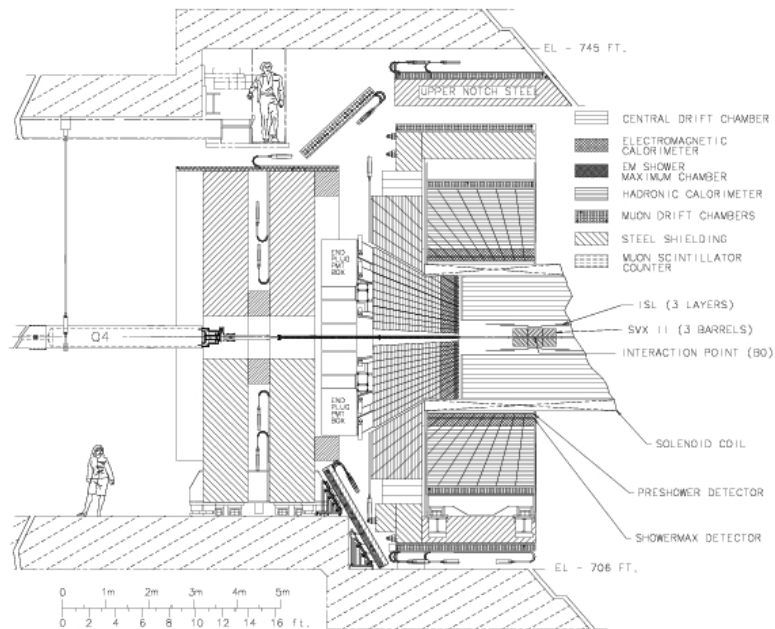


Figure 2: CDF Elevation View

radius and 4.8 m in length, which generates a 1.4 T magnetic field parallel to

the beam axis.

Calorimetry and muon systems are all outside the solenoid.

### 1.2.1 Tracking System

The integrate tracking system is shown in Figure 3.

- At large radii an open cell drift chamber (COT) covers the tracking region  $\eta \leq 1.0$ . Inside the COT, a silicon "inner tracker" is built from two components. A micro-vertex detector at very small radii establishes the ultimate impact parameter resolution. Two additional silicon layers at the intermediate radii provide  $p_T$  resolution in the forward region  $1.0 \leq \eta \leq 2.0$ , and stand-alone silicon tracking over the full region  $|\eta| \leq 2.0$ .

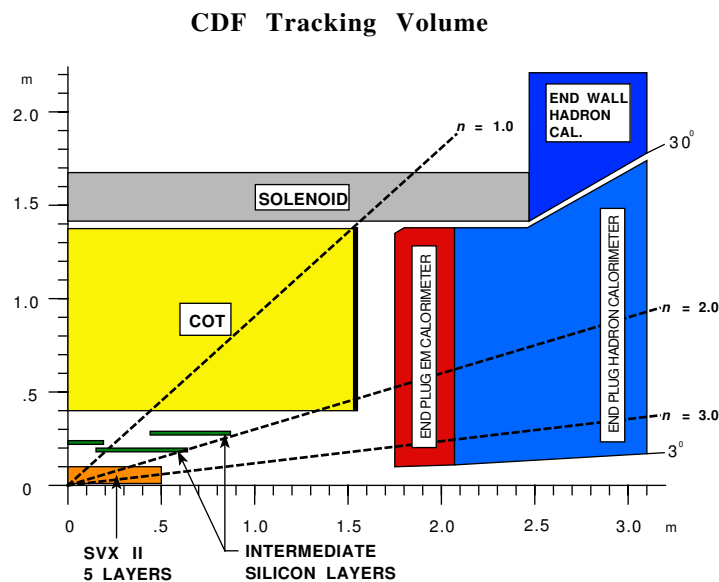


Figure 3: Longitudinal view of the CDF II Tracking System

- Silicon Vertex Detector (SVX II) and Intermediate Silicon Layers (ISL) are both part of Inner Tracker (Figure 4). The silicon vertex detector contains three cylindrical barrels, each barrel supports five layers of double sided silicon microstrip detectors. ISL silicon crystals are mounted in "ladder" assemblies similar to SVX II.

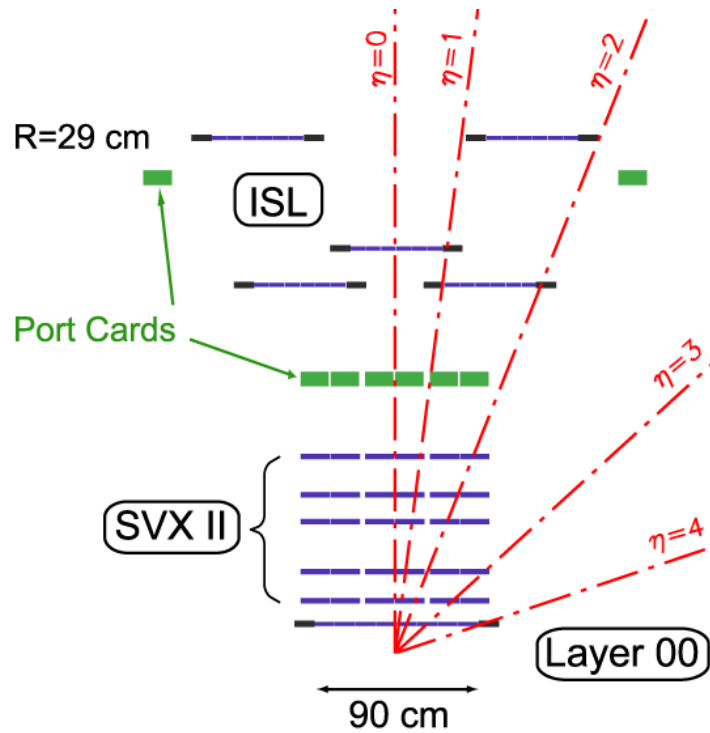


Figure 4: Inner Tracker

### 1.2.2 Calorimeter System

Outside the solenoid, scintillator-based calorimetry covers the region  $|\eta| \leq 1.0$  with separate electro-magnetic and hadronic measurements. In the region  $1.0 \leq |\eta| \leq 3.0$  scintillator-based calorimetry has been replaced, from RUN I, with a scintillating tile plug calorimeter because of the high crossing rates.

### 1.2.3 Muon Systems

CDF II used four systems of scintillators and proportional chambers in the detection of muons over the region  $|\eta| \leq 2.0$ . The absorbers for these systems are the calorimeter steel, the magnet return yoke and additional steel walls.

## 2 W boson

### 2.1 Production and decay

In a  $p\bar{p}$  collider W bosons are produced by the quark anti-quark annihilation. A schematic diagram of the W production process is shown in Figure 5

At  $\sqrt{s} = 1.96 \text{ TeV}$  W bosons are produced mainly by the annihilation of  $u\bar{p}$

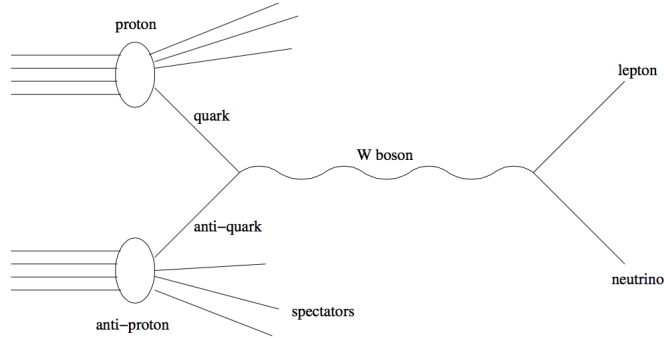


Figure 5: Hadronic W production and its leptonic decay

and *down* quarks.

The inclusive rapidity distribution for production of a  $W^+$  boson in  $p\bar{p}$  collisions is expressed as

$$\frac{d\sigma}{dy_W} = K(y_W) \frac{2\pi G_F}{3\sqrt{2}} x_1 x_2 \{ \cos^2\theta_c (u(x_1)\bar{d}(x_2) + \bar{u}(x_2)d(x_1)) + \sin^2\theta_c (u(x_1)\bar{s}(x_2) + \bar{u}(x_2)s(x_1)) \} \quad (1)$$

where  $G_F$  is the weak coupling constant, the partons from proton (anti-protons) carry momentum fraction  $x_1(x_2)$ , the factor  $K(y_W)$  contains higher-order QCD radiative corrections and PDFs are evaluate at  $Q^2 = M_W$ .

It follows from momentum and energy conservation that  $x_1$  and  $x_2$  satisfy

$$\begin{aligned} M_W^2 &= x_1 x_2 s \\ x_1 - x_2 &= x_W \end{aligned} \quad (2)$$

We know that  $y_W = \ln\left(\frac{E+p_z}{E-p_z}\right) = \ln\frac{x_2}{x_1}$  so

$$x_{1,2} = \frac{M_W}{\sqrt{s}} e^{\pm y_W} \quad (3)$$

This indicates that the momentum fraction of  $u$  and  $d$  quarks are related to the rapidity of produced  $W$ 's.

In a  $p\bar{p}$  collider,  $W$  bosons are reconstructed primarily from their muonic and electronic decay. Hadronic decay is usually buried inside a large QCD background ( $p\bar{p} \rightarrow jets$ ), as are the  $\tau$ 's from the  $W \rightarrow \tau\nu_\tau$  process. In approximately 10% of the  $W$  events, the  $W$  decays into an electron and a neutrino. These are the events which I used in this analysis to measure the  $W$  production charge asymmetry.

The neutrino passes through the detector without interacting. The electron, on the other hand, leaves a track in the tracking chamber, and also deposits its energy in the electromagnetic calorimeter.

## 2.2 Asymmetries

As mentioned in previous section the main  $W$  production at Tevatron is  $u(\bar{u}) - \bar{d}(d)$  annihilation. As shown in Figure 6  $up$  quarks carry a larger fraction of the proton's momentum than  $down$  quarks.

So we can observe an asymmetry in charge of produced  $W$ .

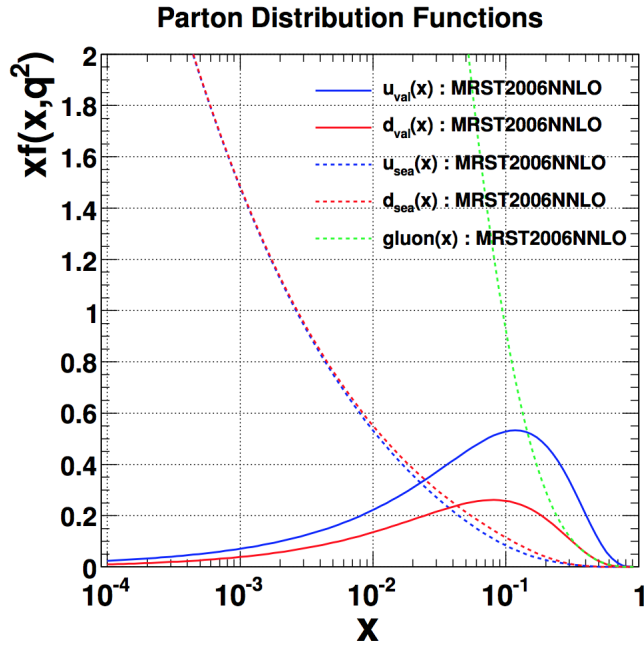


Figure 6: The parton distribution for the proton

In practice, when a  $W^+(W^-)$  is produced it's boosted in the proton ( anti-proton) direction, displayed in Figure 7. Moreover we have to consider special weak current V-A structure which couples only to left-handed quarks

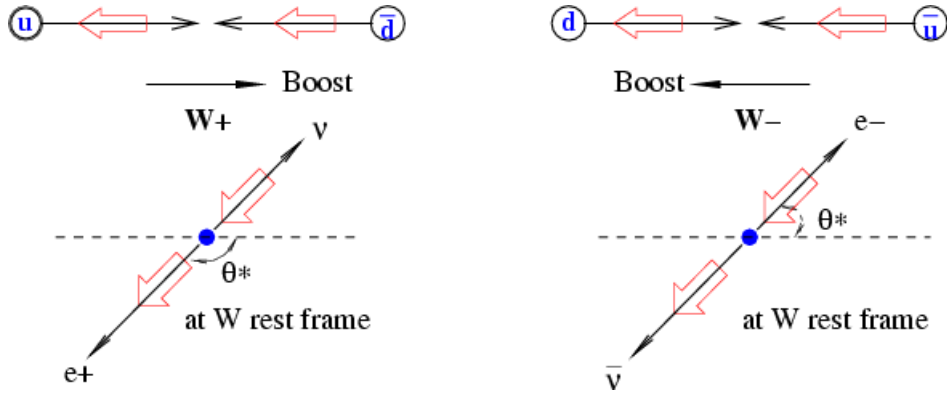


Figure 7: The momenta and helicities in  $p\bar{p} \rightarrow W^\pm$  production and  $W^\pm$  leptonic decay.

and right-handed anti-quarks. For ultra-relativistic quarks this results in full polarization of the produced W bosons in the direction of the beam. The same V-A structure is in decay mode.

So the resulting asymmetry observed detecting leptons is a convolution of these two effects (PDFs of incoming partons and V-A coupling). Since  $u(x_1) = \bar{u}(x_2)$  and  $d(x_1) = \bar{d}(x_2)$  by CPT symmetry, the differential cross sections for W are approximately

$$\begin{aligned} \frac{d\sigma^+}{dy_W} &\approx \frac{2\pi G_F}{3\sqrt{2}} [u(x_1)\bar{d}(x_2)] \\ \frac{d\sigma^-}{dy_W} &\approx \frac{2\pi G_F}{3\sqrt{2}} [d(x_1)\bar{u}(x_2)] \end{aligned} \quad (4)$$

The W production charge asymmetry  $A(y_W)$  in the leading-order parton model is therefore

$$\begin{aligned} A(y_W) &= \frac{d\sigma^+/dy_W - d\sigma^-/dy_W}{d\sigma^+/dy_W + d\sigma^-/dy_W} \\ &\approx \frac{u(x_1)\bar{d}(x_2) - d(x_1)\bar{u}(x_2)}{u(x_1)\bar{d}(x_2) + d(x_1)\bar{u}(x_2)} \end{aligned} \quad (5)$$

There is a direct correlation between the W production charge asymmetry and the  $d/u$  ratio. A precise measurement of the W production charge asymmetry therefore is useful to put constraint on the  $u$  and  $d$  quark momentum distributions. Since the W leptonic decay involves a neutrino, if we would do this measurement by using  $y_W$  we would have to make an assumption on neutrino longitudinal momentum. What we choose is study W charge asymmetry in function of lepton pseudorapidity. The lepton charge asymmetry

is defined as:

$$A(\eta_l) = \frac{d\sigma^+/d\eta_l - d\sigma^-/d\eta_l}{d\sigma^+/d\eta_l + d\sigma^-/d\eta_l} \quad (6)$$

Assuming same acceptance and efficiency for positrons and electrons

$$A^{observed}(\eta_l) = \frac{N^+ - N^-}{N^+ + N^-} \quad (7)$$

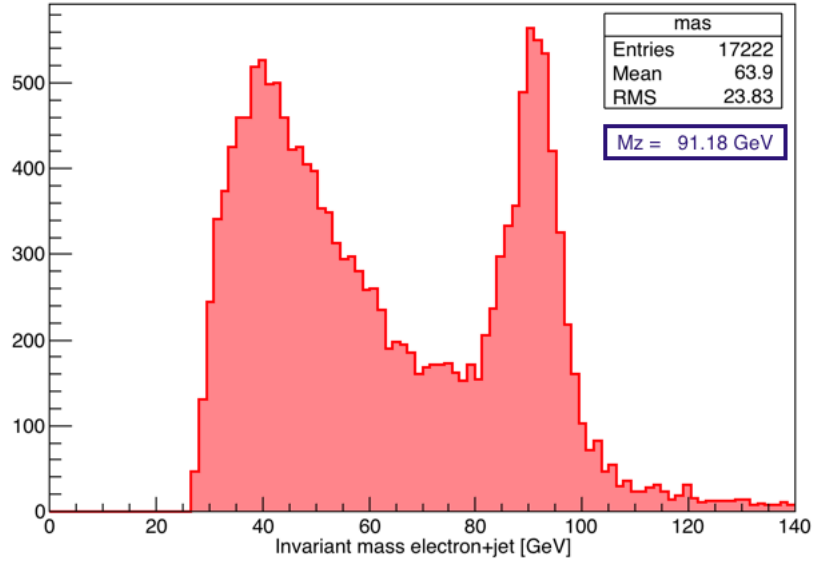
The W charge asymmetry data in  $p\bar{p}$  collisions has an advantage over the determination from proton and neutron structure functions as it is and is free from the kind of uncertainties in nuclear effects that affect the DIS data. This constrain on PDFs is really important for W mass measurement. Improvement in PDF uncertainties will reduce total error on this measurement.

### 2.3 Signal and backgrounds

The process I examined is the general  $W \rightarrow e\nu_e + X$ . At the leading order (LO) experimental signature of  $W \rightarrow e\nu_e$  event is high electron/positron  $E_T$  associated at high  $\cancel{E}_T$  (Missing Transverse Energy). What we should observe is a charged track that fits with electromagnetic shower. This object has to be back-to-back to  $\cancel{E}_T$  in trasverse plan. At the next leading order (NLO) incoming partons could generate hadronic jets by gluons emission. So in the final state we also observe particle shower in hadronic calorimeter. There are several processes that can simulate a  $W \rightarrow e\nu_e$  decay.

- The bigger and harder one is QCD background in which hadron jets are misidentified as electrons. In this case fake electron in hadron jets could came from  $e^+e^-$  pairs, heavy quark decay (bottom or charm quarks) and hadron that fakes electron ( $\pi^\pm$ ).
- $Z \rightarrow e^+e^-$  is also a big background. It could happen that one of two electron from this decays is misreconstructed or goes in dead regions of detector. In Figure 8 it's shown the invariant mass of electron+jet as example of Z's background in central region data sample. This is not an harder background as QCD because is easy to simulate and estimate.
- Also  $Z \rightarrow \tau^+\tau^-$  and  $W \rightarrow \tau\nu_\tau$  are background for this decay channel. In Z's case one  $\tau$  decays in hadrons and the other in leptons so it can easily fake a signal event with an associated jet. Both these background are small and can be estimated by simulation.

Figure 8: Central region, DATA sample



### 3 Data Analysis

In this section I describe all details of my analysis.

#### 3.1 Samples

For this analysis I used several data samples.

- A simulated  $W \rightarrow e\nu_e$  sample, that it's been used to understand signal phenomenology and develop cuts;
- A simulate  $Z \rightarrow e^+e^-$  sample, to better study a know one of the greater background;
- Partial high luminosity data of Run II, in preliminar studies this sample it's been used in comparison with simulated sample. All cuts developed have been applied to this data sample.

Data sample is divided into two parts: events from the central region of the detector and events from the forward region.

## 3.2 General event selections [2] [3] [4]

### 3.2.1 Central events

These events are detected by inner tracker, COT and electromagnetic calorimeter. What we require is high  $p_T$  track that has to match with electromagnetic shower. To do this we plot together simulated and data samples and observe before and after cut distributions shape. Central region events are really clean events because of COT high efficiency. The following selection cuts are made to form the final central W electron sample:

- $E_T \geq 25 \text{ GeV}$ :  $E_T$  is the electron cluster energy transverse to the beam direction

$$E_T = E \sin \theta \quad (8)$$

where E is the cluster energy and  $\theta$  is the polar angle of the associated COT track

- $\cancel{E}_T \geq 25 \text{ GeV}$ :  $\cancel{E}_T$  is the missing transverse energy  $E_T$  in the event defined by

$$\vec{\cancel{E}}_T = -\sum_i E_T^i n_i \quad (9)$$

where  $n_i$  is a unit vector perpendicular to the beam axis and pointing at the center of the  $i^{\text{th}}$  calorimeter tower.

- $E_T^{\text{jet}} \leq 20 \text{ GeV}$ : The  $E_T$  refers to the biggest transverse energy of the jet. The jet is measured in a cone of  $R = 0.7$  (where R is defined as  $\sqrt{(\Delta\phi)^2 + (\Delta\eta)^2}$ ). This reduces the di-jet background in the W sample.
- $LShr \leq 0.2$ : This variable measures the energy sharing between the adjacent towers and the CEM tower with the most of the energy in the electron showers. It is defined as

$$LShr = C \frac{\sum_i (E_i - T_i)}{\sigma} \quad (10)$$

where  $E - i$  = Energy in in Adjacent Towers,  $T_i = E_i$  is the adjacent tower energy as predicted by the measured lateral shower profile at the testbeam and the measure  $z$  location from the CES,  $\sigma_i$  is the combined characteristic fluctuation of the energy excess,  $C$  = Scale Factor = 0.14 and  $i$  is over all the adjacent towers in the electron shower

- $Isolation \leq 0.1$  The isolation variable is a measure of the energy surrounding the electron. It is defined as

$$Isolation = \frac{E_T(R = 0.4) - E_T}{E_T} \quad (11)$$

- $0.5 \leq E/P \leq 2.5$  The ratio of the cluster energy and the momentum of the COT track associated with the energy cluster is required to be consistent with that of a single charged particle. On average this is 1.0 for electrons, but because of the possibility for an electron to radiate photons, there is a long tail in the distribution
- $15 \text{ GeV} \leq P_T \leq 200 \text{ GeV}$ : The transverse momentum is required to be consistent with a W decay electron as well as in a range where the charge can be reliably determined.  $P_T$  is measured relative to the beam line and is determined by the track's curvature in the COT
- $\text{Track } Z_0 \leq 60 \text{ cm}$ : The event vertex is required to be within approximately  $2\sigma$  of the center of the detector
- $E_{Had}/E_{Em} \leq 0.10$

### 3.2.2 Plug Events

Selections on plug region data set are the same than previous case except for the  $E_{Had}/E_{Em}$  selection that is required to be  $\leq 0.05$ .

A good way to see background is to plot isolation in function of missing transverse energy both for simulated then data sample. As we can well

Figure 9: Plug region, DATA sample

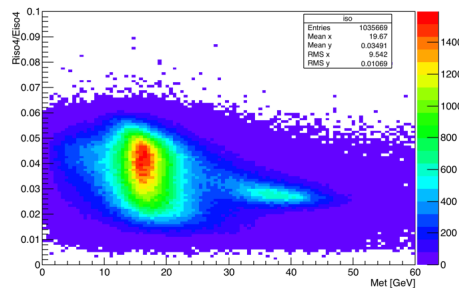
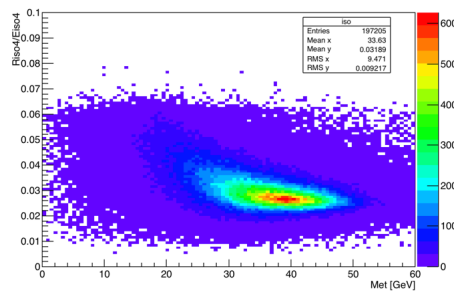


Figure 10: Plug region, SIMULATED sample



notice in Figure 9, the data sample is completely dominated by the background in a very large region. This background region is probably referred to QCD events and it's not completely separated by signal region: as shown in Figure 10 distribution tails seems to be overlapped.

Indeed, in plug region, QCD events dominate data samples.

Historically the  $\cancel{E}_T \geq 25 \text{ GeV}$  selection is also applied on plug region. We decided to study QCD background in the region  $0 \text{ GeV} \leq \cancel{E}_T \leq 25 \text{ GeV}$  to reduce overlapping and then apply this selection cut.

## 4 Plug region special analysis

After applying selections described in the previous section we obtained, for the central region, a relatively background free  $W$  sample. The main reason is that the COT, in addition to Inner Tracker and calorimeter, gives really clean electron candidates. In addition, it happens not so frequently that central region electrons, which track is reconstructed at high radii, are charge misidentified. On the contrary, plug region electrons are only detected by Inner Tracker and electromagnetic calorimeter. In addition charge misidentification problems are not negligible because of small radii track reconstruction. The result is that plug electrons selections described in section 3.2.2 have a big problem: large background in the lower  $\cancel{E}_T$  region. What we have found is that the plug tracks are mostly junk and additional track cleanup is required. Without this additional analysis on plug tracks asymmetry is mostly flat because of dilution by background events.

Requiring clean plug electron selection (section 3.2.2) and splitting missing

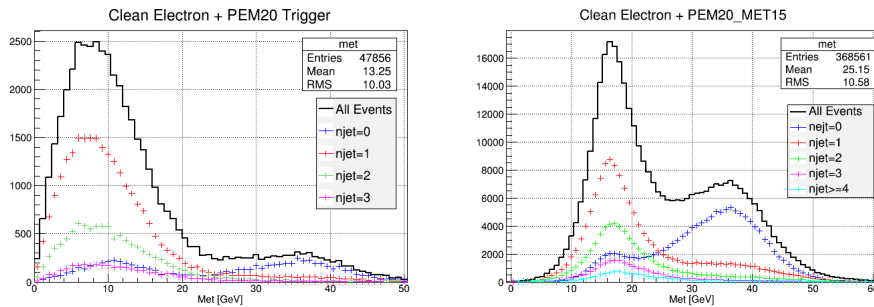


Figure 11:  $\cancel{E}_T$  in function of number of jets in the events for two different triggers

transverse energy distribution in function of number of jet (Figure 11) it's possible to observe background-signal overlapping. Left plot shown  $\cancel{E}_T$  for a PEM20 trigger: because of really high rates this trigger is prescaled at L2

by a factor of 25. Peak around 10 GeV represents mostly QCD background, W signal is the smaller peak around 35 GeV.

The goal of this analysis is to reduce distribution tails of  $n_{jet} \geq 1$  in the signal region so it becomes possible to apply  $E_T \geq 25\text{GeV}$  and obtain a cleaner plug electron sample. The only difference between plot on the left and the one on the right is trigger requirements. It's important to remark that *PEM20\_MET15* trigger is not prescaled and presents resolution effects on 0-20 GeV region.

## 4.1 Good Quality Track selection

There are several reasons for the difficulties in selecting a clean electron sample on plug region. First of all, we have no precise information on vertex because of neutrino in the event.

In addition we have to consider that, at high instantaneous luminosity, there are a lot of secondary interactions and collision point isn't in a small region, as happens now in LHC collisions.

So it could happen that hadronic jets generated at  $z \neq 0$  pass through first SVX II layers and become part of background on data sample.

These reasons explain why we decided to focus our attention on tracking to select a cleaner sample.

Forward tracking utilizes the  $p\bar{p}$  collision vertex, the silicon vertex detector and the plug shower maximum position detector (PES) for tracking space points. Forward tracks are required to pass through 3-8 layers (we are not considering Layer 00) of silicon vertex detector sensors, as shown in Figure 4.

### 4.1.1 Track quality parameters and benchmark distributions

Track quality variables used for this analysis are the following:

- *nsilfid*, this gives the number of silicon layers that the Phoenix track traverses and comes from Phoenix track fiducial layer count function
- *el\_Chi2*, this is the  $\chi^2$  of helix fit
- *el\_NSvxHits*, number of silicon hits on track. There can be more than one hit per silicon layer.

I built a matrix of *el\_Chi2 / numberofhits* for each value of *nsilfid* and *el\_NSvxHits* and then looked at benchmark distributions, listed below:

- *el\_Pem3x3Chi2*, this is the plug 3x3 tower electromagnetic tower shower shape fit  $\chi^2$
- Missing transverse energy distribution

The matrix is used to assess what to reject and what to keep and clean-up with  $el\_Chi2/numberofhits$  cuts. In Figure 12 two examples of matrix

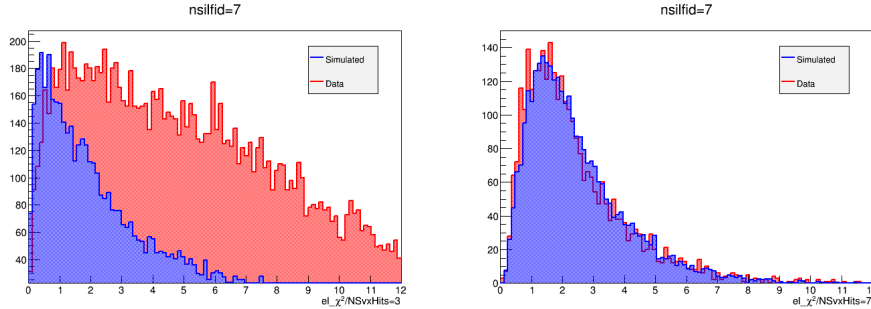


Figure 12:  $el\_Chi2$  for  $nsilfid = 7$  and  $el\_NSvxHits = 3$  (left) and  $el\_NSvxHits = 7$  (right)

elements are shown. On the left rejected case and on the right an approved case. It's important to notice that we choose to rejected cases like the left one because, even putting a stringent cut, a large amount of background events will pass selection.

After looking at all matrix elements what we found is that good cases satisfy:

- $el\_NSvxHits \neq 3$
- $el\_NSvxHits \geq nsilfid$

So all selections are summarized in following table:

$nsilfid \rightarrow$	3	4	5	6	7	8
$nhits = 3$	x	x	x	x	x	x
$nhits = 4$	✓	✓	x	x	x	x
$nhits = 5$	✓	✓	✓	x	x	x
$nhits = 6$	✓	✓	✓	✓	x	x
$nhits = 7$	✓	✓	✓	✓	✓	x
$nhits \geq 8$	✓	✓	✓	✓	✓	✓

Final step has been to study final benchmark distributions shapes and apply final selection cut.

In Figure 13  $el\_Pem3x3Chi2$  distribution are shown. After matrix elements study, cut down on the right has been applied. Final missing transverse energy distribution are in Figure 14 Now for  $njet \neq 0$  tails are smaller in signal region and PEM20\_MET15 plot shows how background peak has been strongly reduced in comparison with starting status (Figure 11).

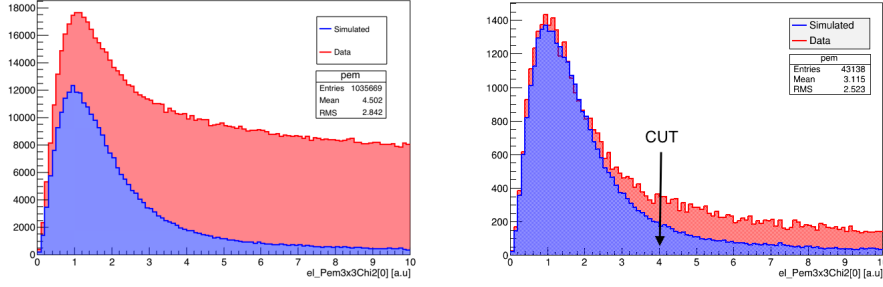


Figure 13:  $el\_Pem3x3Chi2$  before any kind of selection cut (left) and after good quality matrix selection (right)

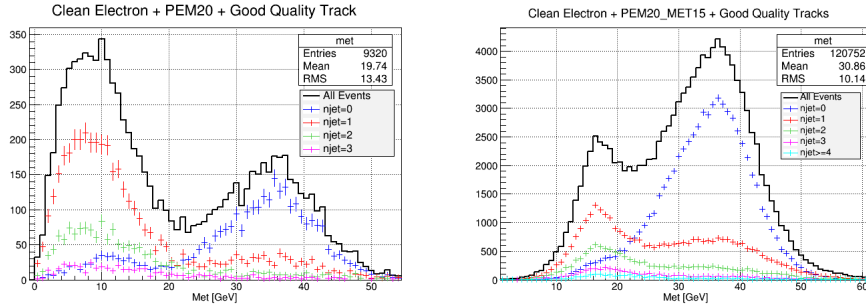


Figure 14:  $\cancel{E}_T$  in function of number of jets in the events for two different triggers AFTER MATRIX SELECTION AND  $el\_Pem3x3Chi2$  CUT

## 5 Asymmetry plots and results

Thanks to the good quality selection on plug electron data sample, described in Section 4, and final  $\cancel{E}_T \geq 25$  GeV cut, it has been possible to work on asymmetry plots without any background dilution effect.

For plug region we require events to pass PEM20\_MET15 trigger. Asymmetry has been defined in Section 2.2, Equation 7. Uncertainty on each point is

$$\sigma_{A(\eta)} = \frac{1 - A(\eta)^2}{N^+ + N^-} \quad (12)$$

As we can see in Figure 15, because of background high rate, if no cuts are applied asymmetry is close to zero (left plot). Looking at same figure, the right plot shows what's selection results on data sample. There are some high statistic fluctuations if  $\eta$  is close to  $|1|$  because of really low acceptance of detector (dead region). It's also possible to observe charge misidentification effects in high  $\eta$  regions of asymmetry. In the end of this section details about this phenomena will be briefly described.

Because of CP invariance it's possible to combine negative and positive

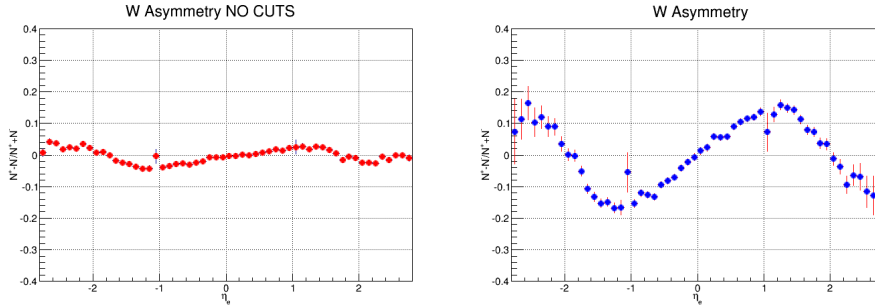


Figure 15: Asymmetry in function of electron  $\eta$  before and after selection cuts

pseudorapidity counting and plot W Asymmetry in function of  $|\eta|$ , as done in Figure 16.

In this case problems referred to dead region of detector are almost solved,

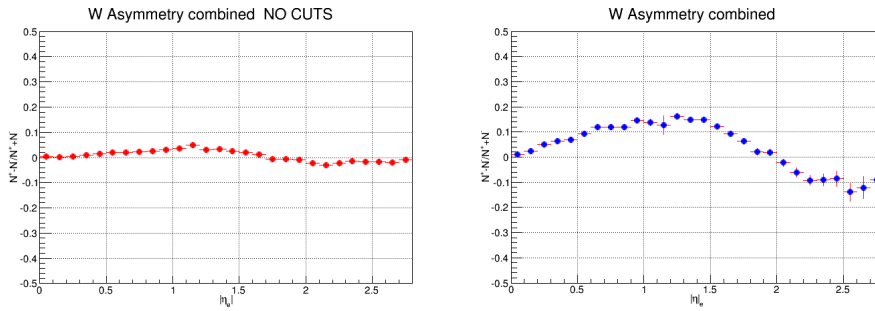


Figure 16: Asymmetry Combined in function of electron  $\eta$  before and after selection cuts

but charge misidentification problem are still visible in high  $|\eta|$  value region. Our result is also consistent with previous measurement at Low Instantaneous Luminosity as shown in Figure 17 and Figure 18

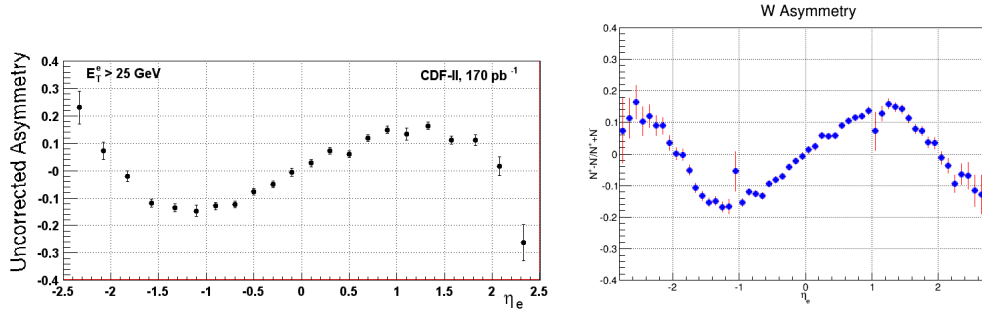


Figure 17: Low Instantaneous Luminosity vs High Luminosity Raw Asymmetry

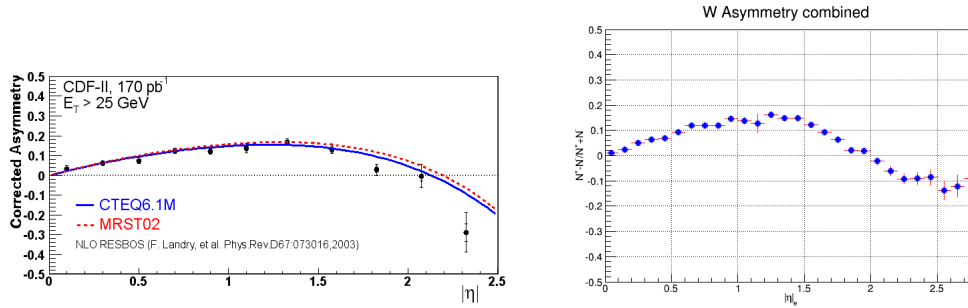


Figure 18: Low Instantaneous Luminosity vs High Luminosity Raw Combined Asymmetry

## 5.1 Charge Misidentification [5]

As already explained the electron identification is constructed, and observed, to have a charge symmetric efficiency. However, resolution effects can lead to misidentification of the charge, which dilutes the asymmetry. Residual misalignments in the silicon detector and calorimeters could give rise to a bias in the charge identification that would directly bias the asymmetry. It's possible to define the corrected asymmetry in function of probability to mis-identify an electron and a positron. A good check could be done using a  $Z \rightarrow e^+e^-$  sample.

This kind of study takes a lot of time, so we only focused on analysis technique shown previously.

Preliminary study on charge misidentification helped us to better understand problem in high pseudorapidity region. I report plots obtained. The general idea is to study the  $\Delta\phi$  at the PES exit radius between the infinite momentum (curvature = 0) value of  $\phi$  and the one with the finite curvature from the track helix in function of  $|\eta_{det}|$ . There are two finite curvature  $\phi$ 's at the

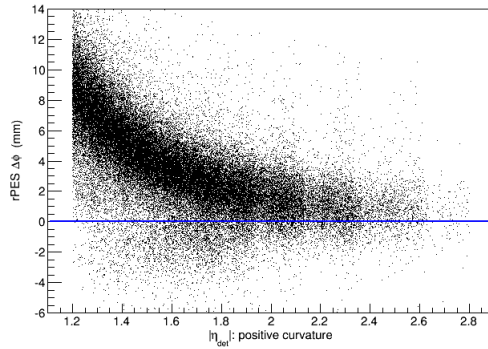


Figure 19: Measured bend Plane  $r\Delta\phi$  (Positive curvature)

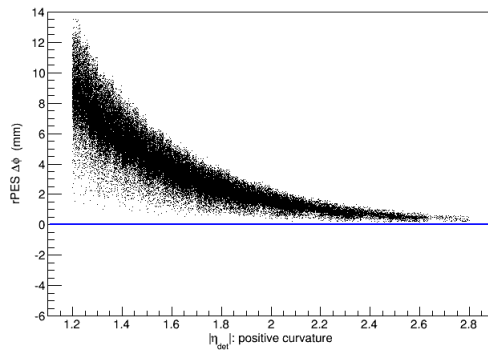


Figure 20: Prediction from track helix bend Plane  $r\Delta\phi$  (Positive curvature)

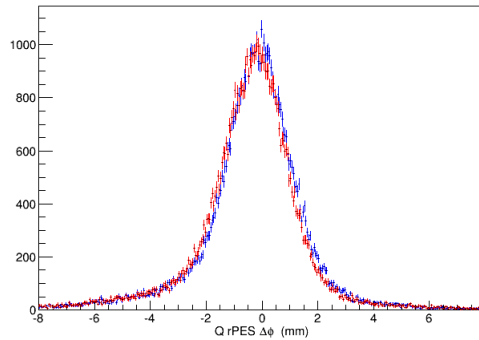


Figure 21:  $\Delta\phi$  between measured and predicted  $\phi$  at PES exit radius

PES exit: measured and track helix extrapolated  $\phi$ . In Figure 19 and 20 is shown the the  $rPES\Delta\phi$  or track bend offset at the PES exit radius. Measure  $\phi$  includes measurement resolution plus  $p_T$  distribution. The points under

zero offset for  $|\eta_{det}|$  between 1.4 and 2 appear to be from tracking screw-ups, not resolution.

These are nice plots that give a qualitative sense of the level of charge misID vs  $|\eta_{det}|$ . In Figure 21  $\Delta\phi$  between measured and predicted  $\phi$  at PES exit radius. In this graph blue represents and red the negative one. Asymmetry in this plot shape is referred to bremsstrahlung effects and curvature differences.

## 6 Conclusions

- We studied all possible background of  $W \rightarrow e\nu$  channel and focused on the bigger one: QCD background
- We checked that central region data are really good and they don't need special studies.
- Plug region events had a large amount of background in the lower  $\cancel{E}_T$  region.
- We developed quality track cut algorithm before  $Met \geq 25$  GeV cut
- Raw Asymmetry at High Luminosity seems to fit with Low Instantaneous Luminosity measurement.  
**We succeeded!**
- More study on charge misidentification are needed.

## References

1. The CDF II Detector: Technical Design Report, *The CDF II Collaboration*, October 1996;
2. Measurement of the W Boson Production Charge Asymmetry in  $p\bar{p}$  collisions, Bo-Young Han, 2008;
3. Measurement of the Forward-Backward Charge Asymmetry from  $W \rightarrow e\nu$  Production in p anti-p Collisions at  $\sqrt{s} = 1.96$  TeV (arXiv:hep-ex/0501023);
4. Measurement of the electron charge asymmetry in  $p\bar{p} \rightarrow W \rightarrow e\nu + X$  events at  $\sqrt{s} = 1.96$  TeV, (arXiv:/0807.3367)
5. <http://b0urpc.fnal.gov/willis/urelog/wasym0/cdf1790.pdf>, Track helix reference, *Hans Wenzel*